Applied Catalysis B: Environmental 331 (2023) 122668

Contents lists available at ScienceDirect

Applied Catalysis B: Environmental

journal homepage: www.elsevier.com/locate/apcatb

Cryptomelane nanowires for highly selective self-heating photothermal synergistic catalytic oxidation of gaseous ammonia

Yu Zhou [a,1], Yanfang Feng [b,1], Huifang Xie [a], Jingling Lu [a], Danni Ding [a], Shaopeng Rong [a,*]

[a] Jiangsu Key Laboratory of Chemical Pollution Control and Resources Reuse, School of Environmental and Biological Engineering, Nanjing University of Science and Technology, Nanjing 210094, China

[b] Key Laboratory of Agro-Environment in Downstream of Yangtze Plain, Key Laboratory of Integrated Planting and Breeding, Ministry of Agriculture and Rural Affairs, Institute of Agricultural Resources and Environment, Jiangsu Academy of Agricultural Sciences, Nanjing 210014, China

ARTICLE INFO

Keywords:
Photothermal catalysis
Thermalcatalysis
Cryptomelane
Mechanism
Ammonia

ABSTRACT

Photothermal selective catalytic oxidation of NH_3 (NH_3-SCO) provided a cost-effective approach to controling NH_3 pollution. However, the contribution of photocatalysis and thermalcatalysis in photothermal NH_3-SCO, as well as the synergistic mechanism was not well addressed. Herein, the cryptomelane nanowires were developed for self-heating photothermal NH_3-SCO, and excellent NH_3 conversion (91.7%) and N_2 selectivity (94.7%) were achieved. Furthermore, the study of the synergistic mechanism showed that the photothermal NH_3-SCO can be attributed to the thermal-assisted photocatalytic mechanism, which is the synergy of photocatalysis and photothermal effect. Moreover, the reaction paths of photothermal and thermal NH_3-SCO were comparative studied. For the photothermal NH_3-SCO, it is considered to follow the photo-iSCR mechanism, in which the activation of NH_3 into $\bullet NH_2$ by photogenerated holes serves a key role; while the thermalcatalysis is mainly dominated by the iSCR mechanism and supplemented by the imide mechanism. This research provides fundamental insights into the photothermal NH_3-SCO mechanism.

1. Introduction

Ammonia (NH_3) is one of the frequent pollutants in indoor and outdoor air, which not only leads to various environmental problems, but also seriously affects human health. Since NH_3 is the primary alkaline gas in the atmosphere, which can combine with NO_x or SO_2 to produce ammonium nitrate or ammonium sulfate particles, respectively. These particulate matter precursors are incredibly crucial to the early nucleation of aerosols and the development of secondary particles throughout the heavy haze pollution process [1]. In addition, NH_3 will also cause soil and surface water acidification and water eutrophication through atmospheric nitrogen deposition, and finally interfere with the nitrogen balance in the ecosystem [2]. Moreover, NH_3 volatilization is the most important form of nitrogen loss during fertilization, which is also the emission gas with the greatest environmental impact during the production of organic fertilizers. On the other hand, as one of the main sources of indoor air pollution, NH_3 has been listed as a toxic substance by the U.S. National Institute for Occupation Safety and Health (NIOSH) [3]. In the past years, more emphasis has been placed on eliminating formaldehyde and VOCs [4–6]; while ignoring the harm of indoor NH_3. NH_3 is usually released from fly ash mortar in construction materials, cementitious materials containing urea, frost protection agent, and human respiration and sweat [7,8]. The excess emission of NH_3 can be extremely harmful to human health such as breathing difficulties, eye infections, pulmonary edema, diabetes, and even death [9]. In accordance with regulations of NIOSH, the maximum limit for human exposure to NH_3 is 25 ppm for 8 h, and the limit of short-term exposure is 35 ppm for 15 min [9]. Hence, there is an urgent need for practical application to develop a suitable catalyst that can convert NH_3 into harmless N_2. To date, developing catalysts with much higher NH_3 removal rate and N_2 selectivity is still a great challenge.

Thermalcatalysis and photocatalysis strategies perform an imperative role in the selective catalytic oxidation of NH_3 (NH_3-SCO). Noble metals and transition metal oxides are the two primary types of catalysts used in the thermalcatalytic oxidation of NH_3. Noble metal catalysts supported with Pt, Pd, Ru, Au and Ag usually exhibit excellent low-temperature NH_3 oxidation activity [10]. However, because of its strong oxidation performance, noble metal catalysts are easy to over

* Corresponding author.
E-mail address: rongrsp@njust.edu.cn (S. Rong).
[1] These authors contributed equally to this paper.

https://doi.org/10.1016/j.apcatb.2023.122668
Received 10 January 2023; Received in revised form 10 March 2023; Accepted 19 March 2023
Available online 21 March 2023

oxidize part of NH_3 to NO_x, resulting in low N_2 selectivity. Despite the high activity of noble metals at low temperatures, their scarcity and relatively low N_2 selectivity make them difficult to apply on a large scale [11]. Transition metal catalysts are mainly Cu, Fe, Mn, Co and V based catalysts, especially Cu-based catalysts, which can give consideration to both oxidation activity and selectivity [10–13]. In addition to Cu-based catalysts, Mn-based catalysts also exhibit much higher NH_3-SCO activity [10]. For instance, Qu et al., found that MnO_2 prepared by urea-assisted synthetic method exhibited higher NH_3-SCO activity, which could achieve complete conversion of NH_3 at 170 °C [14]. It was found that the lower reduction temperature, abundant NH_3 adsorption sites, more oxygen vacancies and surface active oxygen species lead to relatively excellent NH_3-SCO activity of Mn-based catalysts. Our previous publication [15] reported a kind of layered MnO_2 with strengthened by surface acidic sites, which exhibited much lower complete NH_3 conversion temperature and higher N_2 selectivity. Research found that the improvement in NH_3-SCO activity was mainly due to the abundant surface active oxygen species and enhancement of acidic sites. Particularly, it was the Brønsted acidic sites that not only serves as adsorption sites, but also as reaction sites, which facilitate the adsorption, activation and further oxidation of NH_3. In general, thermalcatalytic removal of NH_3 usually requires much higher temperatures and is difficult to apply in practical applications for indoor NH_3 removal. Besides the thermalcatalysis, in recent years, photocatalysis has gradually started to be applied to the removal of gaseous NH_3. For instance, Chen et al. prepared different exposed facets (i.e. {001}, {101} and {010}) of anatase TiO_2 to evaluate its performance in photocatalytic oxidation of NH_3, and found that the {001} facets showed optimal activity [16]. In addition, traditional visible-light-sensitive NH_3 oxidation catalysts (N-TiO_2, g-C_3N_4 and Ag_3PO_4) were tested and found that the semiconductor Ag_3PO_4 can achieve room-temperature NH_3 oxidation under visible light [17]. Nevertheless, the NH_3-SCO efficiency of most photocatalysts is still unsatisfactory, and higher optical power is also required.

In response to these problems, photothermal catalysis, which combines the photochemical and thermochemical effects of solar-light, has emerged as a rapidly growing and exciting research area [18,19]. Compared with single photocatalysis or thermalcatalysis, photothermal synergistic catalysis can not only take advantage of the two reaction driving forces of light energy and heat energy at the same time, but also enhance the reaction rate through the synergistic effect. Photothermal catalysis is not a simple superposition of photocatalysis and thermalcatalysis, but a synergy effect. At present, according to the action mechanism of photothermal catalytic materials, photothermal synergistic catalysis mainly includes two categories: (1) light and heat act on the bifunctional catalyst at the same time to produce the synergistic effect; (2) light and heat act on photocatalyst and thermalcatalyst respectively, and produce synergy through material coupling. However, most of the previously reported photothermal synergistic catalysis require external heat sources or composite thermal response components to drive the thermal catalytic reaction. Although the reaction activity can be improved, it will inevitably increase additional energy consumption or reduce the utilization efficiency of light energy. Therefore, the development of self-heating photothermal synergistic catalytic materials with solar-light driven photocatalysis and self-heating thermalcatalysis will be a promoting strategy. Manganese oxides, including cryptomelane, exhibit strong absorption in the entire spectrum range and show excellent photothermal conversion effect [18]. Moreover, some literature [20], including our previous publication [21], also confirmed that the cryptomelane has certain photocatalytic activity and can generate electron-hole pairs with irradiation of solar-light. Therefore, the cryptomelane with excellent photo absorption, photothermal effect and certain photocatalytic activity has become a potential ideal material for photothermal NH_3-SCO. For the synergetic mechanism, photothermal catalysis is not just a simple superposition of photocatalysis and thermalcatalysis. Currently, there are three mechanisms adopted in literature to explain thermalcatalytic oxidation of NH_3 [10–13]: (1) the imide intermediate mechanism; (2) the hydrazinium-type intermediate mechanism; (3) in-situ or "internal" selective catalytic reduction (iSCR) mechanism. Although thermalcatalysis and photocatalysis mechanism for NH_3 have a certain understanding, the reaction mechanism of photothermal catalytic oxidation has not been definitively established. On the one hand, the process and mechanism of photothermal catalytic oxidation of NH_3 are not clear. The contribution and function of photocatalysis and thermalcatalysis in photothermal catalysis, as well as the more important synergistic mechanism also need to be further explored.

In this contribution, the cryptomelane nanowires were prepared, and its NH_3-SCO activity and N_2 selectivity were further evaluated by self-heating photothermal synergistic catalytic oxidation. Subsequently, the process and mechanism of photothermal and thermal catalytic oxidation of NH_3 are comparatively explored. Furthermore, the contribution of photocatalysis and thermalcatalysis, as well as the more important synergistic mechanism were also discussed. This may be the first report on self-heating photothermal synergistic catalytic oxidation of NH_3 via cryptomelane, and achieved excellent catalytic activity and selectivity. This study deepens insight into photothermal synergistic catalysis and is of great significance to the purification of other indoor toxic air pollutants.

2. Experimental section

2.1. Catalysts preparation

2.1.1. Synthesis of the cryptomelane

The cryptomelane was controllable prepared based on a hydrothermal redox method. During a typical synthesis, 25 mmol of $KMnO_4$ and 10 mmol of $(NH_4)_2C_2O_4{\cdot}H_2O$ were dissolved in 70 mL of deionized water with vigorous magnetic stirring. After that, the uniformly mixed solution was poured into a stainless-steel autoclave with a Teflon liner containing 100 mL. Subsequently, the autoclave was transferred to an electric oven and maintained at 180 °C for 24 h. Finally, the precipitate was collected using filtration after the autoclave had gradually cooled to room temperature, rinsed several times with deionized water, and then dried at 105 °C.

2.1.2. Synthesis of control catalysts

A series of semiconductor catalysts were synthesized as a control group. All these control catalysts (g-C_3N_4 [17], Ag_3PO_4 [17,22], P25 and TiO_2-001 [16,23]) were papered according to previous references, and the specific preparation process can be found in Supporting Information.

2.2. Catalysts characterization and evaluation of NH_3-SCO activity

The details of methods and instruments for catalyst characterization are all presented in Supporting Information. The evaluation of NH_3-SCO activity was conducted in a fixed-bed flow quartz tube reactor equipped with a quartz window (Fig. S1), and the detailed evaluation process can be available in Supporting Information.

3. Results and discussion

3.1. Physicochemical characterization

The cryptomelane was obtained using a feasible hydrothermal redox reaction of $KMnO_4$ and $(NH_4)_2C_2O_4{\cdot}H_2O$. The X-ray diffraction pattern in Fig. 1a confirmed a pure α-MnO_2 structure without any other impurity phases. In fact, the cryptomelane type MnO_2 is a mineralogical name, the crystal structure of cryptomelane type MnO_2 is consistent with α-MnO_2. The crystal structure of α-MnO_2 consists of 2 × 2 co-sided octahedral MnO_6 chains, the chains are connected to each other by oxygen atoms at the vertices of octahedral MnO_6, forming a one-dimensional pore channel of approximately 0.46 nm × 0.46 nm

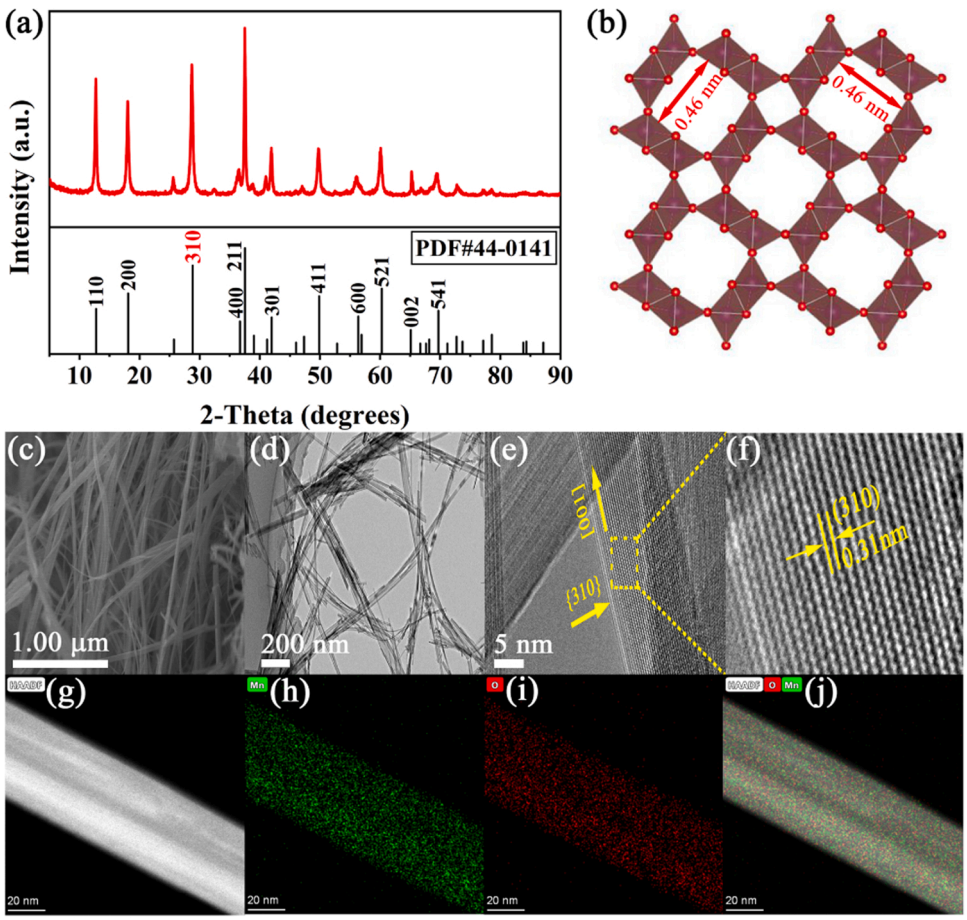

Fig. 1. (a) XRD pattern, (b) atomic structure, (c) SEM image, (d) TEM and (e, f) HRTEM images, (g) HAADF-STEM image and (h-j) corresponding EDX elemental mapping images of as-prepared cryptomelane.

(Fig. 1b). SEM image in Fig. 1c indicates that as-prepared cryptomelane exhibits the morphology of nanowires. TEM also confirmed the nanowire morphology of the cryptomelane (Fig. 1d), and its lattice distance along the [001] direction is 0.31 nm, matching the {310} facets of α-MnO_2 (Fig. 1ef). Furthermore, high angle annular dark field image scanning transmission electron microscope (HAADF-STEM) was also preformed to observe the morphology of the cryptomelane (Fig. 1g), and the corresponding energy dispersive X-ray spectroscopy (EDX) elemental mapping images revealed the distribution of Mn and O (Fig. 1h-j). In addition, it was found that cryptomelane owned a relatively high specific surface area (102.72 m^2/g). On the other hand, in the insert graphic of Fig. 2a, it can be found that there are two peaks, one is an obvious peak located at 10 nm and the other is relatively weak in the range of 4–6 nm. It suggests that the pore size of cryptomelane is mainly distributed at about 10 nm. Furthermore, the chemical formulation of cryptomelane was gained according to element analysis and thermogravimetric analysis. In particular, the H_2O content of the material is calculated by thermogravimetric analysis, and the recorded weight at an early stage is assumed to be the elimination of H_2O from the material (Fig. S2). The results of element analysis show that the K/Mn (ICP-OES) and O/Mn (XPS) are 0.23 and 1.96, respectively. The thermogravimetric analysis shows that the water content is 3.78%. Based on the above results, the chemical composition of cryptomelane can be calculated as $K_{0.23}MnO_{1.96}{\cdot}0.21H_2O$. Since the surface chemical states play a significant role in the catalytic process, the surface composition of cryptomelane was investigated by X-ray photoelectron spectroscopy (XPS). As presented in Fig. 2b, the Mn $2p_{3/2}$ peak is deconvoluted into two peaks, 641.0–641.2 and 642.3–642.4, which are allocated to Mn^{3+} and Mn^{4+}, correspondingly [24]. From the quantitative calculation of the Mn species, it is clear that the Mn^{3+}/Mn^{4+} ratio reached 0.81. Moreover, the average oxidation state (AOS) of Mn can be calculated based on the magnitude of the Mn 3 s multiplet splitting using the empirical formula, i.e. AOS = 8.956 – 1.126 × △E. The △E in Fig. 2c is 4.79, and the corresponding AOS is calculated as 3.56. Besides, the O 1 s spectra can be divided into two peaks (Fig. 2d), which represent surface adsorbed oxygen (O_{ads}) and lattice oxygen (O_{latt}), respectively. The analytical results of XPS spectra imply that cryptomelane has much more O_{ads}, and its O_{ads} to O_{latt} ratio can be up to 0.60.

3.2. Photothermal synergistic catalytic oxidation of ammonia

The photothermal synergistic catalytic activity of cryptomelane with irradiation of simulated solar-light was investigated. As shown in Fig. S3, the cryptomelane exhibited efficient activity across the full solar spectrum light with a 91.7% conversion of NH_3. In particular, in addition to the high NH_3 conversion, the cryptomelane also exhibited much higher selectivity, approaching 95%. Moreover, the rapid return of NH_3 concentration to its initial value in the dark field after switching off the solar-light further confirmed that photothermal catalytic oxidation, not adsorption, should be responsible for the elimination of NH_3 when exposed to solar-light. To learn more about the specific parameters affecting the photothermal catalytic performance of NH_3, the effects of space velocity, optical power density and optical wavelength on the NH_3 conversion and N_2 selectivity were detailed studied. As displayed in Fig. 3a, it is evident that as space velocity increases, the photothermal catalytic oxidation efficiency of NH_3 drops dramatically. While at the same time, the N_2 selectivity also tends to decline significantly. The NH_3 conversion at an airspeed of 200 $L/g_{cat}{\cdot}h$ is only 18.9%, which is just

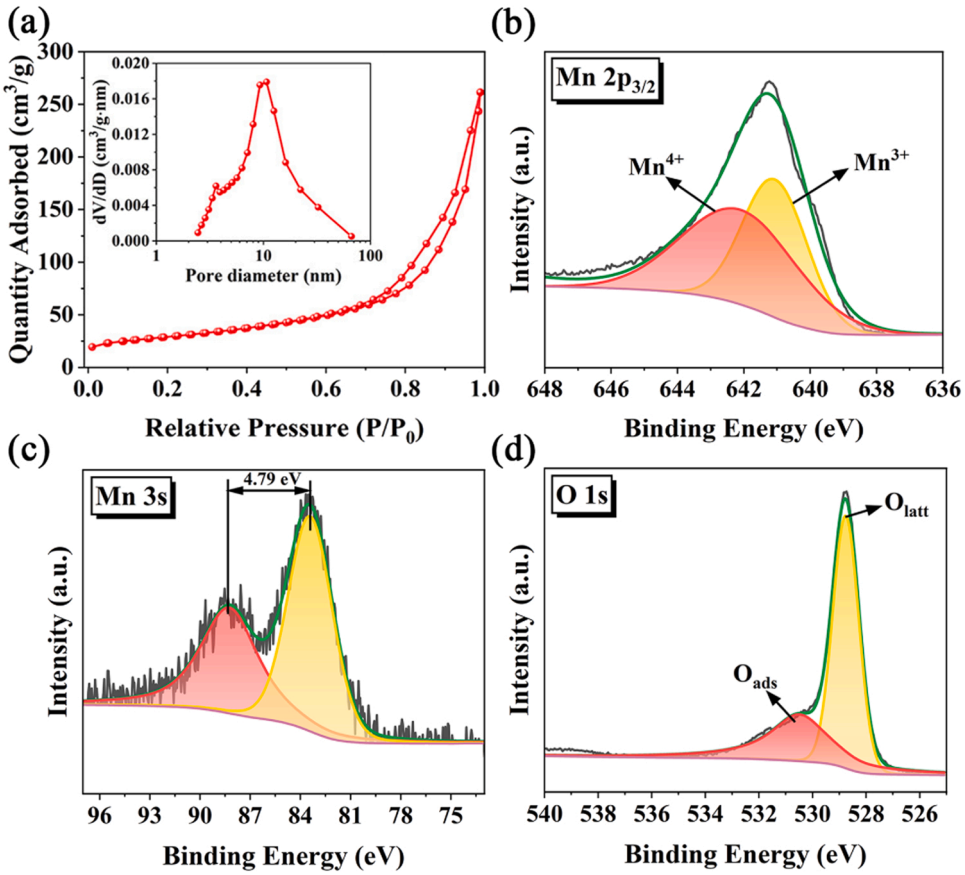

Fig. 2. (a) N_2 adsorption-desorption isotherms and the insert graphic shows the pore size distributions of cryptomelane; XPS spectra of cryptomelane: (b) Mn $2p_{3/2}$, (c) Mn 3s, (d) O 1s.

approximately 20% of that at airspeed of 60 L/g_{cat}·h. Additionally, the effect of optical power densities on the photothermal catalytic efficiency of cryptomelane was investigated. It can be found that the NH_3 conversion is significantly affected by optical power density, which is almost linearly related to the optical power density (Fig. 3b). Correspondingly, the N_2 selectivity gradually improves with the increase of optical power density and remains at a high level. Theoretically, the wavelength of light has an important influence on the photochemical reaction process. The photothermal catalytic oxidation performance of NH_3 with irradiation of different wavelength light was studied by setting various cutoff filters (visible light, > 400, > 470, > 550, > 630 nm). As shown in Fig. 3c. the photothermal catalytic conversion of NH_3 was 91.7%, 39.0%, 40.9%, 29.6%, 12.2% and 7.3% under the irradiation of full spectrum, visible light, and visible infrared irradiation at wavelengths above 400, 470, 550 and 630 nm. respectively. Notably, even under visible light irradiation, cryptomelane still exhibited a high photothermal catalytic activity of up to 39% and the N_2 selectivity can still be maintained above 82% (Fig. S4). In general, operating parameters, such as space velocity, optical power density and optical wavelength, not only have a significant effect on NH_3 conversion, but also present a certain effect on N_2 selectivity.

The NH_3 photothermal catalytic oxidation performance of cryptomelane was also compared with a series of common photo-response catalysts reported in the literature (Fig. 4a-e). The NH_3 conversion of g-C_3N_4, Ag_3PO_4, P25, and TiO_2-001 were 13.3%, 17.1%, 35.5%, 45.7%, respectively, which was significantly lower than 91.7% of the cryptomelane. Besides, it is also very evident in that the photothermal catalysis of cryptomelane is more selective for N_2 than the other four commonly used photo-response catalysts. These results show that cryptomelane exhibits high catalytic activity and selectivity under irradiation containing full spectrum and visible-infrared light. In addition, the NH_3-SCO activity of various catalysts obtained in this study and reported in the literature related to photothermal and photo NH_3-SCO was summarized in Table S1. Herein, it should be noted that the literature related to thermal NH_3-SCO was not listed. On the one hand, the research of synergy mechanism in Section 3.3 has confirmed that the photothermal NH_3-SCO of cryptomelane can be attributed to the thermal-assisted photocatalytic mechanism, in which photocatalysis is the major process of NH_3 elimination; On the other hand, some reviews have made a good summary of thermal NH_3-SCO [10,12,13]. The summary in Table S1 also confirms that the cryptomelane reported in this study exhibits excellent NH_3-SCO activity, much better than most catalysts reported in the literature. Furthermore, the photothermal catalytic oxidation cyclability and stability of the cryptomelane for NH_3 were also assessed. A recyclability analysis revealed that there was no obvious inactivation of cryptomelane even after successive on-off lamp reactions (Fig. 4f), demonstrating good catalytic durability of cryptomelane.

3.3. Mechanism of photothermal synergistic catalytic oxidation of ammonia

To date, the photothermal catalysis mechanism is still controversial and can be broadly interpreted as three modes: one is synergistic catalysis of photocatalysis and thermalcatalysis; the second is light-driven thermalcatalysis mode; and the third is thermally assisted photocatalysis mode. Therefore, it is extremely meaningful to reveal the mechanism of photothermal catalytic oxidation of NH_3, as well as the contribution of photocatalysis and thermalcatalysis. Manganese oxides, due to its remarkable full spectrum absorption characteristics, exhibit significant photothermal conversion effects [25,26]. On the one hand,

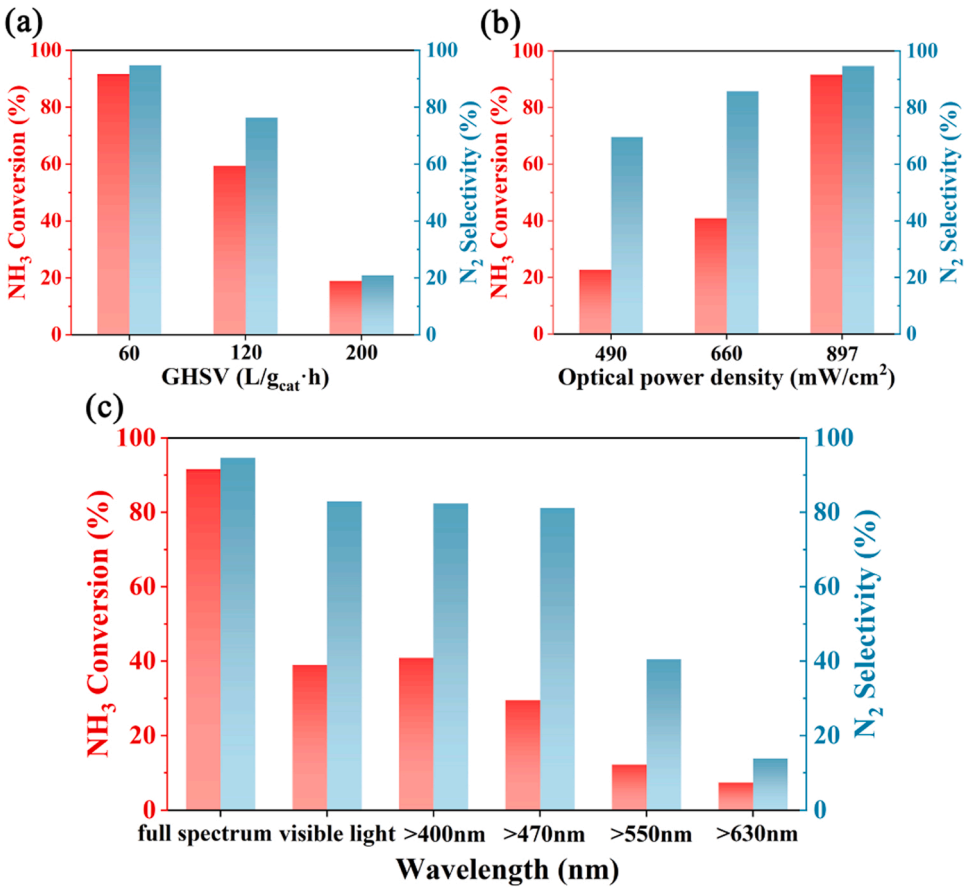

Fig. 3. NH_3 conversion and N_2 selectivity over cryptomelane with (a) different gas hourly space velocity (GHSV), (b) optical power density and (c) wavelength.

with continuous solar-light radiation, the surface temperature of the cryptomelane will increase significantly; on the other hand, the cryptomelane also has high thermalcatalytic activity at low temperature. Therefore, some researchers have suggested that the efficient catalytic performance of cryptomelane under solar-light irradiation comes from light-driven thermal catalysis [25]. To verify this hypothesis, we have tested the surface temperature of cryptomelane at different optical power densities using a thermocouple temperature probe. With continuous solar-light radiation of 490, 660 and 897 mW/cm^2, the surface temperature of the cryptomelane will gradually increase and finally stabilize at 45, 51 and 69 °C, respectively (Fig. S5). Cryptomelane can almost completely remove NH_3 with irradiation of 897 mW/cm^2 solar-lighr, and the corresponding surface temperature is 69 °C. However, it can be clearly found from the insert of Fig. 5 that the cryptomelane exhibits almost no thermalcatalytic activity for NH_3 under the same experimental conditions. Therefore, we can exclude the possibility that the excellent photothermal catalytic performance of cryptomelane is due to light-driven thermocatalysis. In addition, the thermocatalytic oxidation performance of cryptomelane at various temperatures was also tested. In Fig. 5, it is noteworthy that its thermocatalytic activity starts at a low temperature of 120 °C and reaches almost complete conversion at 170 °C. At the same time, its selectivity to N_2 increases significantly with the rise of temperature, exhibiting more than 93% N_2 selectivity at the complete conversion temperature. All the above results demonstrate cryptomelane exhibits fabulous catalytic activity and high selectivity in both photothermal catalytic and thermocatalytic oxidation of NH_3.

In addition to thermalcatalytic activity, our previous studies also found that the cryptomelane also has excellent photocatalytic activity [21]. Firstly, UV–vis–IR absorption spectra was measured and it was observed that cryptomelane has strong absorption in the entire solar-light region from 200 to 2500 nm (Fig. 6a), which is far superior to photocatalytic materials such as g-C_3N_4, Ag_3PO_4, P25(TiO_2), TiO_2-001 [17,27,28]. For photocatalysis, the band gap energy is also an important factor, the narrow band gap is conducive to electron transition and produce more photogenerated carriers. The band-gap energy (E_g) of cryptomelane was measured from Tauc diagrams of diffuse reflectance spectral conversion. As shown in Fig. 6b, the E_g of cryptomelane is 1.51 eV, which is advantageous for its small band gap energy compared to TiO_2 (3.0–3.2 eV) [17]. More electrons are excited by light to leap across the band gap from the valence band (VB) to the conduction band (CB), resulting in more production of electron-hole pairs, which greatly contribute to the excellent photocatalytic oxidation performance. In addition, the photocurrent response of cryptomelane under simulated solar-light irradiation was detected by several ON-OFF cycles of light (Fig. 6c). Its good sensitivity to light is the basis for the effective separation of its electron-hole pairs. In general, the experimental results and literature sufficiently confirmed the photocatalytic activity of the cryptomelane. According to the above discussion, we have first excluded the light-driven thermocatalysis mechanism. Therefore, photocatalysis should be responsible for the remarkable catalytic activity of cryptomelane under solar-light irradiation. Rui's group [29–31] has also carried out a lot of research related to photothermal catalysis and also revealed the photothermal synergistic mechanism. Research showed that, at the low-temperature region, photocatalysis plays a major role in photothermal catalytic VOCs oxidation. Only when the temperature is high enough can thermalcatalysis become the dominant mechanism. Therefore, Rui's research conclusion about the photothermal synergistic mechanism is similar to ours, in which the photocatalytic process is the dominant mechanism of photothermal NH_3-SCO.

However, the function of self-heating generated from photothermal conversion in the photothermal synergistic catalysis needs to be further

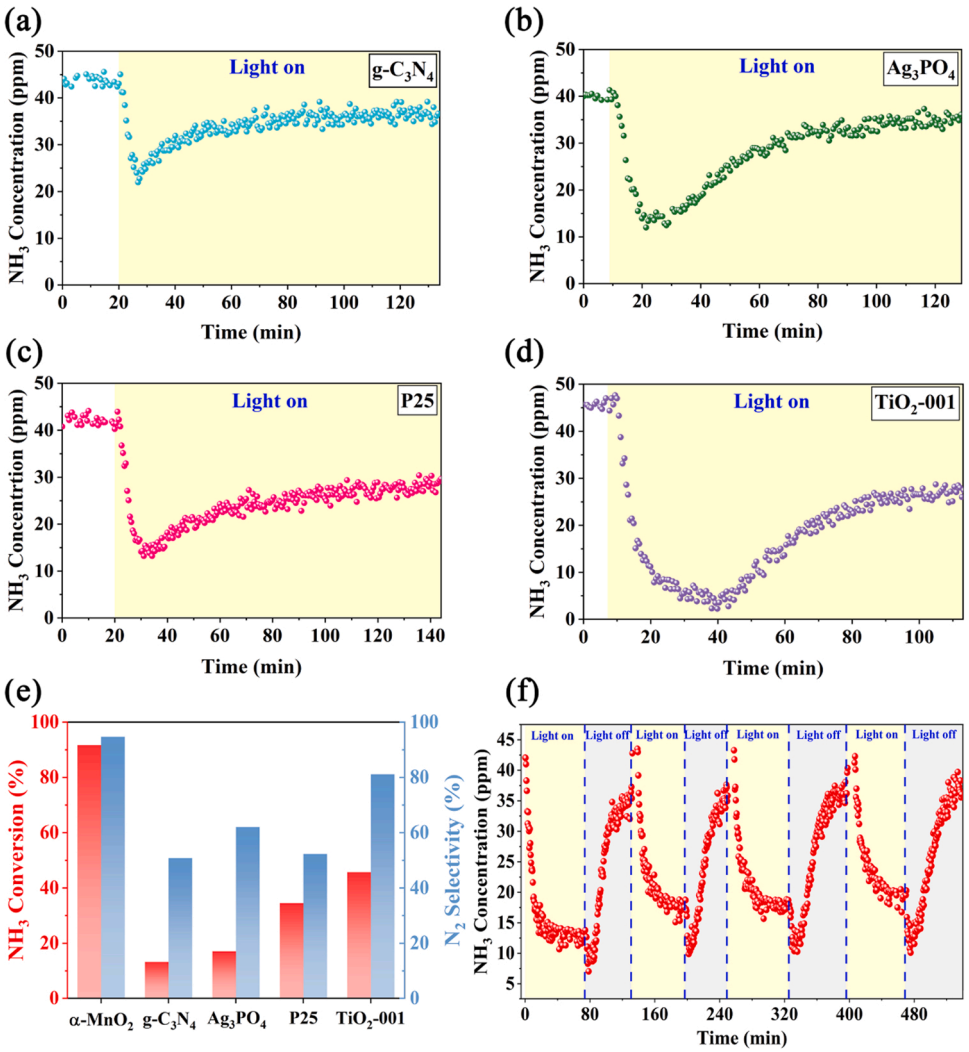

Fig. 4. Photothermal catalytic oxidation of NH_3 over (a) g-C_3N_4, (b) Ag_3PO_4, (c) P25 and (d) TiO_2-001 with irradiation of simulated solar-light. (e) NH_3 conversion and N_2 selectivity over α-MnO_2, g-C_3N_4, Ag_3PO_4, P25, TiO_2-001 with irradiation of simulated solar-light; (f) Cyclability testing of cryptomelane under four consecutive light and dark fields.

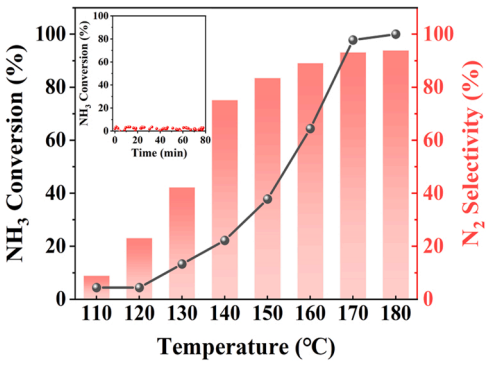

Fig. 5. NH_3 conversion and N_2 selectivity over cryptomelane at different temperature; The insert graphics shows the NH_3 conversion over cryptomelane at 69 ℃ (NH_3 concentration = 45 ppm, 21%O_2, N_2 as balance gas, RH = 38%).

explored. In order to further investigate the photothermal catalytic oxidation mechanism, we conducted temperature-controlled tests in the photothermal oxidation of NH_3 on cryptomelane. As illustrated in Fig. 7, when the reaction temperature was controlled at 25 °C, the NH_3 conversion was only 42.8%, a decrease of more than half compared to the temperature-uncontrolled photothermal catalytic process (self-heating temperature reaches 69 °C). To further verify the effect of temperature, the same activity evaluation was carried out with the temperature controlled at 5 °C, and the results showed that the conversion was only 25.9%. It should be noted that cryptomelane hardly exhibits thermal-catalytic activity of NH_3 with temperature below 120 °C in dark field. Therefore, the above phenomenon proves that temperature plays an important role in the photothermal catalytic process. In other words, the catalytic activity of cryptomelane under solar-light radiation does not only come from photocatalysis alone. In conclusion, the photothermal catalytic oxidation of NH_3 over cryptomelane can be attributed to the thermal-assisted photocatalytic mechanism, that is, the synergy of photocatalysis and photothermal effect. Furthermore, the thermal-assisted effect on photocatalytic process can be summarized into the following two aspects. On the one hand, the oxygen exchange between the lattice oxygen and the ambient oxygen is sped up when manganese dioxide is heated, which makes it easier for the substrates to be oxidized by photocatalysis [18,32]. During the oxygen exchange process, oxygen vacancies are usually generated in situ. The presence of oxygen vacancies introduces intermediate energy levels within the band gap of manganese dioxide, which can narrow the band gap and facilitate the transition of electrons from VB to CB, and finally promotes the efficiency of electron hole separation. Discussion in Section 3.4 has confirmed that

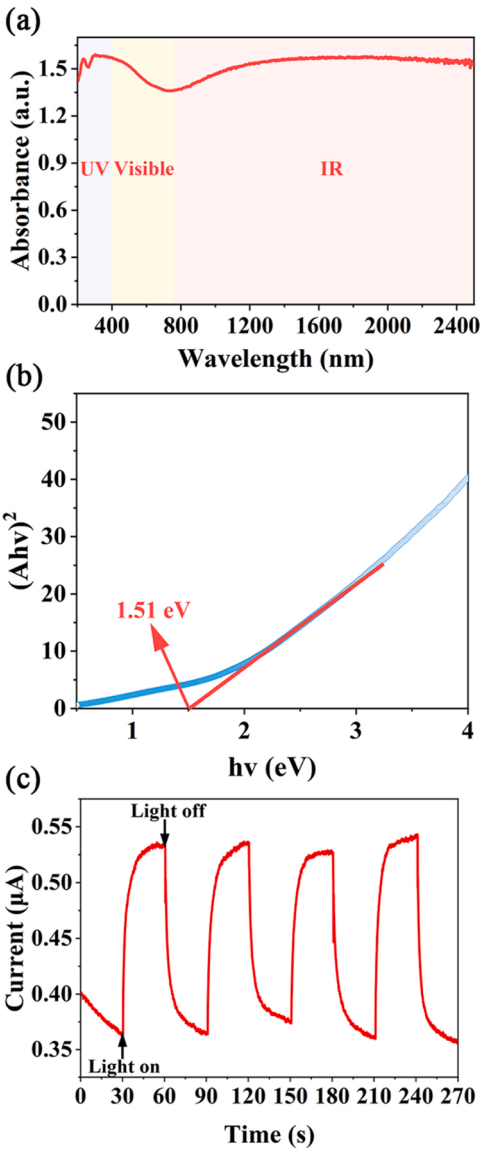

Fig. 6. (a) UV–vis–IR DRS spectra of cryptomelane; (b) Tauc plot of $(Ah\nu)^2$ versus energy $h\nu$ for the indirect band gaps of cryptomelane; (c) Photocurrent transient response of cryptomelane under simulated solar-light.

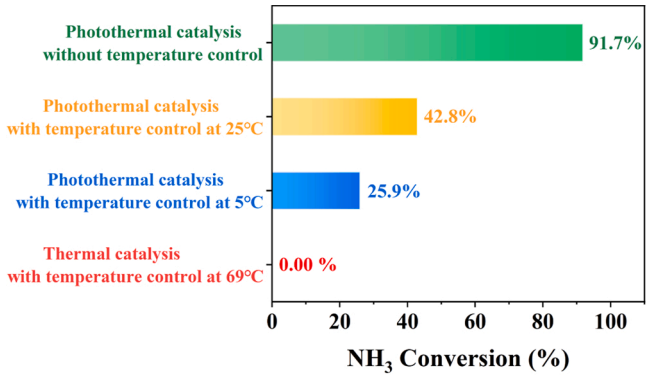

Fig. 7. Photothermal and thermal catalytic activity of cryptomelane under the different constant temperature.

the photoexcited holes take a decisive position in the NH_3 oxidation (NH_3 to $\bullet NH_2$). Thus, there is no doubt that promoting photogenerated holes can improve the activity of photocatalytic oxidation of NH_3. On the other hand, previous research has claimed that light radiation can enhance the lattice oxygen activity of manganese dioxide [25], which is conducive to the conversion of lattice oxygen into surface active oxygen. The d-d orbital electrons of the Mn atom in [MnO_6] octahedron can absorb photon energy and transit from the ground state to the excited state when exposed to solar-light irradiance, resulting in the weakening of the Mn-O bond and the strengthening of lattice oxygen activity. While surface active oxygen plays a significant role in the second step of photocatalytic oxidation of NH_3 ($\bullet NH_2$ to NO, NO_2, NO_3^-). Therefore, increasing the temperature is conducive to enhancing the activity of lattice oxygen, produce more surface-active oxygen, and accelerate the further oxidation of NH_3.

3.4. *Photothermal catalytic and thermocatalytic mechanism of NH_3-SCO*

To further reveal the pathway of photothermal catalytic oxidation of NH_3 over cryptomelane, in-situ DRIFTS was used to probe the changes of intermediate species. As shown in Fig. 8a, cryptomelane was first pretreated under nitrogen atmosphere without light irradiation, and then the mixture of NH_3/O_2 was introduced with the irradiation of simulated solar-light. A series of peaks at 1245 cm^{-1}, 1370 cm^{-1}, 1445 cm^{-1}, and 1553 cm^{-1} were observed, and its intensity increased gradually with the extension of the exposure time, suggesting the process of photothermal catalytic oxidation of NH_3 on cryptomelane. The bands at 1245 cm^{-1} and 1370 cm^{-1} are attributed to the ligand NH_3 bound to the Lewis acid center and the ionic NH_4^+ bound to the Brønsted acid center, respectively [33]. Furthermore, the spectral bands (1445 cm^{-1}) of ionic NH_4^+ are gradually enhanced and adsorbed on the catalyst surface, indicating that new Brønsted acid sites formed from M-NO_2 nitro compounds (NH_xNO_y) [34]. The bands at 1553 cm^{-1} correspond to the nitrate species, which is due to the adsorption of the intermediate species NO_x generated in the photothermal catalytic oxidation of NH_3. Besides, the negative absorption bands at 3415 cm^{-1} are ascribed to the surface hydroxyl group, which is the result of NH_3 adsorption on the cryptomelane surface through hydrogen bonding [35].

As for the photocatalytic decomposition of NH_3, some literature indicates that it may follow the photo-iSCR mechanism [16,17,33,34,36], in which the activation of NH_3 into $\bullet NH_2$ by photogenerated holes is the key step. As discussed in Section 3.3, the photothermal catalytic oxidation of NH_3 can be attributed to the thermal-assisted photocatalytic mechanism, which is the synergy of photocatalysis and photothermal effect. Photocatalysis is the major mechanism in the photothermal catalytic oxidation of NH_3, it is speculated that the photothermal catalytic oxidation of NH_3 on cryptomelane may also conform to photo-iSCR mechanism. In the photo-iSCR mechanism, the first step, that is the activation of NH_3 into $\bullet NH_2$ by photogenerated holes, serves a pivotal role in the photocatalytic of NH_3. In order to confirm the activation process and the role of photogenerated holes, electron paramagnetic resonance (EPR) and radical scavenger were utilized. As shown in the insert graphic of Fig. 9, compared to the dark conditions, an additional signal at $g = 1.986$ due to $\bullet NH_2$ generation was detected under solar-light irradiation. It suggests that photogenerated holes produced on cryptomelane under solar-light irradiation can oxidize NH_3 into $\bullet NH_2$. Furthermore, potassium oxalate monohydrate ($K_2C_2O_4{\cdot}H_2O$) was used as an scavenger for hole trapping experiments [34]. The results in Fig. 9 indicate that the presence of photogenerated holes scavenger significantly inhibited the oxidation of NH_3, leading to a significant decrease in NH_3 conversion from 91.7% to 19.6%. It suggests that photogenerated holes play an indispensable role in the activation of NH_3 to $\bullet NH_2$ and the subsequent oxidation process. Combining the results of in-situ DRIFTS and EPR, the following reaction steps are proposed as possible mechanisms for the photothermal catalytic oxidation of NH_3 over cryptomelane. As shown in Fig. 10, NH_3 is first adsorbed onto the

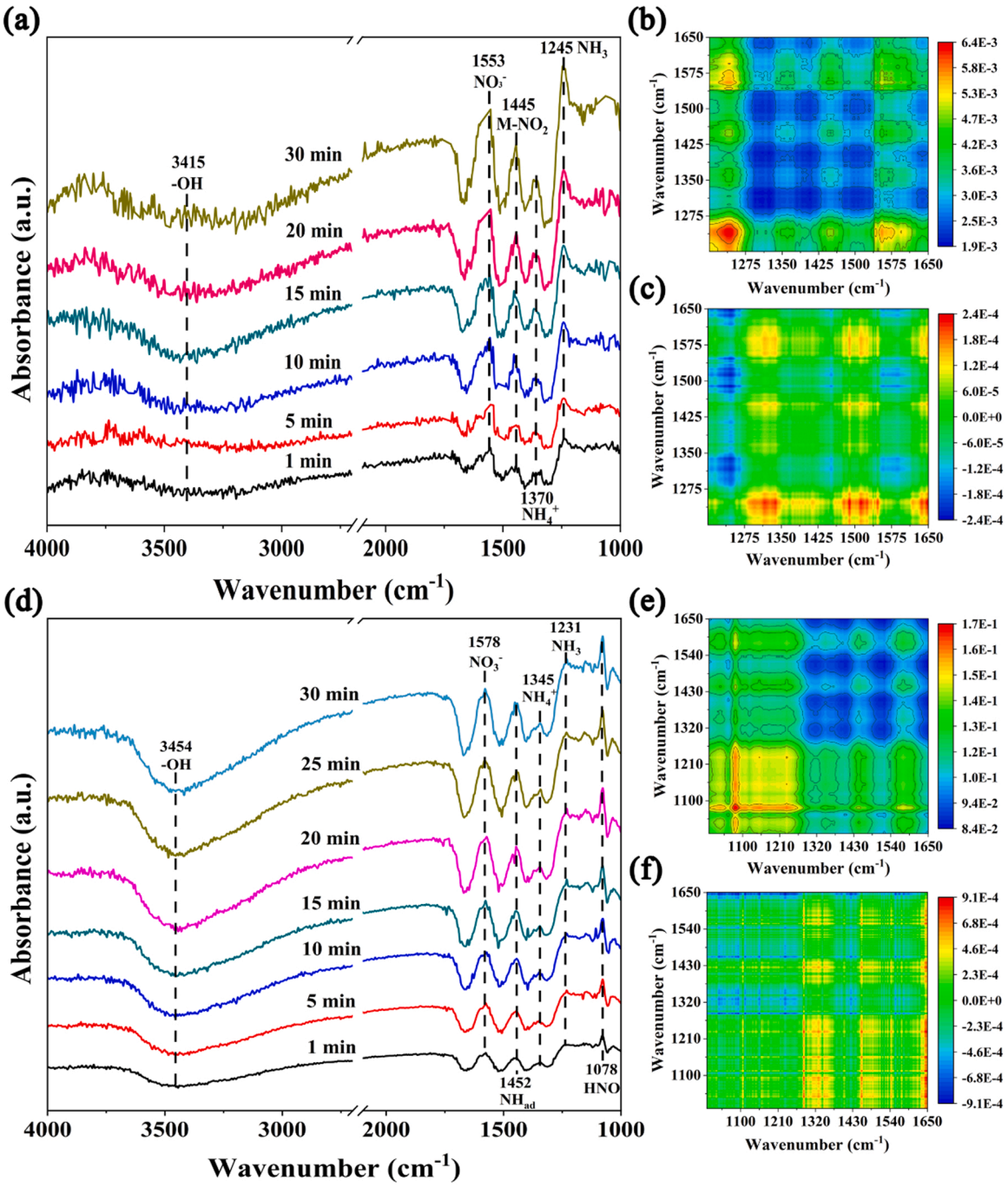

Fig. 8. *In-situ* DRIFTS of (a) photothermal catalytic oxidation of NH_3 over cryptomelane; (b) Synchronous and (c) asynchronous two-dimensional correlation analysis of in-situ DRIFTS of photothermal catalytic oxidation of NH_3 over cryptomelane; (d) *In-situ* DRIFTS of thermalcatalytic (160 °C) oxidation of NH_3 over cryptomelane; (e) Synchronous and (f) asynchronous two-dimensional correlation analysis of in-situ DRIFTS of thermalcatalytic oxidation of NH_3 over cryptomelane.

Lewis acid sites and the Brønsted acid sites as coordinated NH_3 and ionic NH_4^+, correspondingly. When cryptomelane is excited by solar-light, electron-hole carriers are generated and migrate to the cryptomelane surface. Subsequently, the photogenerated holes will oxidize NH_3 into $\bullet NH_2$; $\bullet NH_2$, as a pivotal specie, will combine with active oxygen species (such as $\bullet O_2^-$, $\bullet OH$) to produce the intermediate NO_x or further NO_3^-; the in situ generated NO_x will be further reduced by $\bullet NH_2$ and/or NH_3 to finally produce N_2. The reaction sequence of this mechanism can be further confirmed by the synchronous and asynchronous two-dimensional correlation analysis of the in-situ DRIFTS (Fig. 8bc), which presents an increase in the intensity of the nitrate peaks at 1553 cm^{-1} before the M-NO_2 nitro compounds (NH_xNO_y) at 1445 cm^{-1}, implying that nitrate is produced first and then reacts further to produce M-NO_2. In the photo-iSCR mechanism, the first step, that is the activation of NH_3 into $\bullet NH_2$ by photogenerated holes, serves a pivotal role in the photocatalytic of NH_3.

For the thermalcatalytic oxidation of NH_3 reaction pathways on metal oxides have been investigated and described in recent papers [10, 37]. The main mechanisms of thermalcatalytic oxidation include the imide intermediate (-NH) mechanism, the hydrazinium-type intermediate (N_2H_4) mechanism and in situ selective catalytic reduction (iSCR) mechanism. To explore the mechanism followed by NH_3 on cryptomelane, in-situ DRIFTS of thermalcatalytic oxidation of NH_3 was also carried out. After pretreatment of the sample, NH_3 and O_2 were introduced

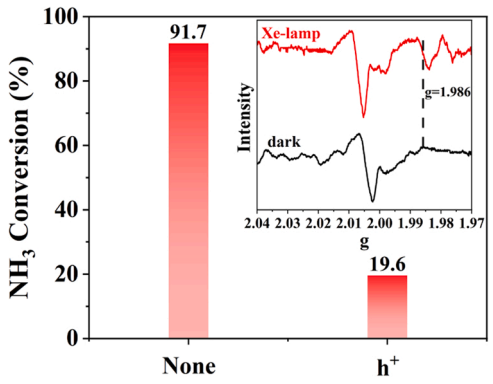

Fig. 9. The capture experiment of active species h^+ during photothermal catalytic oxidation of NH_3; The insert graphic is the EPR spectra of cryptomelane after pre-adsorption of NH_3.

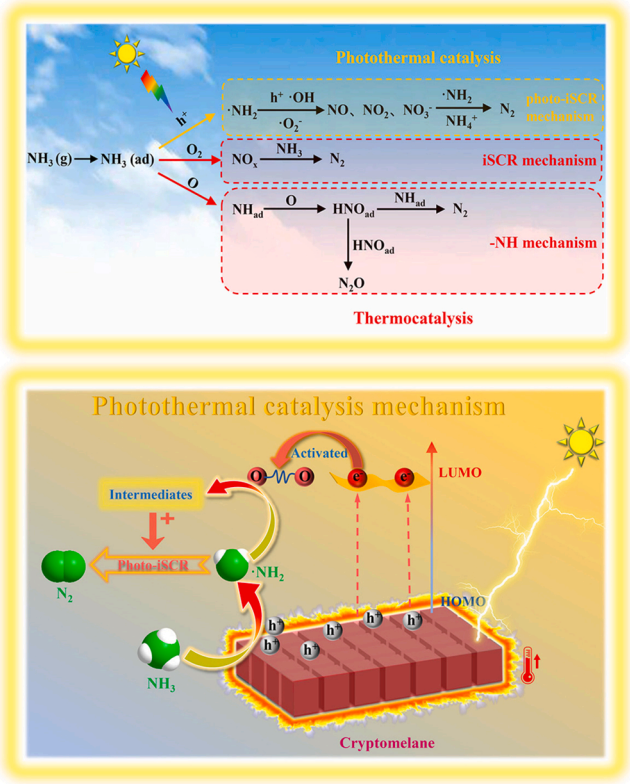

Fig. 10. Mechanisms of photothermal catalytic and thermalcatalytic oxidation processes of NH_3 over cryptomelane.

at 160 °C and several peaks were evident at 1078 cm^{-1}, 1231 cm^{-1}, 1345 cm^{-1}, 1452 cm^{-1} and 1578 cm^{-1} (Fig. 8d). The bands at 1078 cm^{-1} are attributed to NH deformation in HNO, together with bands at 1231 cm^{-1} ascribed to coordinate NH_3 combined with Lewis acid center. The bands at 1345 cm^{-1} are assigned to the NH_4^+ species bound by the Brønsted acid center. While the bands observed at 1452 cm^{-1} are peaks caused by the NH_{ad} species [37,38]. The generation of HNO and NH_{ad} as key intermediates confirms that the thermalcatalytic oxidation of NH_3 on cryptomelane follows the imide mechanism. In addition, distinct nitrate bands appear at 1578 cm^{-1}, and nitrate can again react with the introduced NH_3, which is consistent with the iSCR mechanism. The above findings indicate that there is not only one reaction mechanism for the thermocatalytic oxidation of NH_3 on cryptomelane, but the imide mechanism and the iSCR mechanism coexist. As for the thermalcatalytic oxidation process (Fig. 10), NH_3 adsorbed on cryptomelane first reacts with O_2 to form NO_x, which can be proved by the intermediate of nitrate produced in the in-situ reaction (Fig. 8d); then the in-situ generated NO_x can react with NH_3 to form N_2, which confirms that the thermalcatalytic process follows the iSCR mechanism. Notably, intermediates HNO and NH_{ad} were also observed from the in-situ reaction of NH_3 and O_2, suggesting that there is more than one reaction mechanism for NH_3 oxidation on cryptomelane. With HNO as the key intermediate in the imide mechanism, we believe that the surface adsorbed NH_3 can also react with reactive oxygen species to generate intermediate NH_{ad}, which can be further oxidized by reactive oxygen species to HNO; and then HNO in turn react with the generated NH_{ad} to produce N_2. According to the analysis of Fig. 8ef, for the change order of intermediate species in the reaction of the imide mechanism, the strength of NH_{ad} at 1452 cm^{-1} increases earlier than that of HNO at 1078 cm^{-1}, which once again verifies our reasoning on the reaction of the imide mechanism. Meanwhile, the in-situ reaction of NH_3 oxidation in Fig. 8d shows that the peak intensity of intermediate nitrate is significantly higher than that of intermediate HNO, which further explains that the thermocatalytic oxidation on cryptomelane mainly follows the iSCR mechanism.

Taking the above results into account, it can be found that the mechanism of photothermal and thermal catalytic decomposition of NH_3 on cryptomelane is significantly different. For photothermal NH_3-SCO, it is considered to follow the photo-iSCR mechanism, in which the activation of NH_3 into $\bullet NH_2$ by photogenerated holes is the key step in the NH_3 photocatalytic oxidation. While the reaction pathway of thermal NH_3-SCO is mainly dominated by the iSCR mechanism and supplemented by the imide mechanism. The different NH_3 oxidation paths between photothermal catalysis and thermalcatalysis result in a remarkable distinction in NH_3-SCO activity.

4. Conclusion

In conclusion, the cryptomelane nanowires were prepared for self-heating photothermal synergistic catalytic oxidation of NH_3 with the irradiation of solar-light. The cryptomelane exhibited excellent NH_3-SCO across the full solar spectrum light with a 91.7% conversion of NH_3 and a 94.7% N_2 selectivity, which are much superior to those of common photo-response catalysts (e.g., g-C_3N_4, Ag_3PO_4, P25, TiO_2-001). Results of the synergistic mechanism revealed that the NH_3 photothermal catalytic oxidation of cryptomelane can be attributed to the thermal-assisted photocatalytic mechanism. The reaction path of NH_3 oxidation by thermalcatalysis and photothermal catalysis were also compared. For photothermal catalytic oxidation, it is considered to follow the photo-iSCR mechanism. The activation of NH_3 into $\bullet NH_2$ by photogenerated holes is the key step in the NH_3 photothermal catalytic oxidation. While the reaction pathway of thermalcatalysis is mainly dominated by the iSCR mechanism and supplemented by the imide mechanism. This research provides novel insights into the mechanism of photothermal synergistic catalytic oxidation of NH_3 over MnO_2-based catalysts.

CRediT authorship contribution statement

Yu Zhou: Investigation, Methodology, Writing – original draft, Visualization. **Yanfang Feng:** Supervision, Methodology, Writing – review & editing, Methodology. **Huifang Xie:** Supervision, Methodology. **Jingling Lu:** Visualization, Formal analysis. **Danni Ding:** Methodology, Investigation. **Shaopeng Rong:** Supervision, Writing – review & editing, Conceptualization, Project administration, Funding acquisition.

Declaration of Competing Interest

The authors declare that they have no known competing financial interests or personal relationships that could have appeared to influence

the work reported in this paper.

Data Availability

Data will be made available on request.

Acknowledgment

This work was financially supported by the Natural Science Foundation of Jiangsu Province (No. BK20221496), National Natural Science Foundation of China (No. 21906084) and "333" High-level Talents Training Project of Jiangsu Province (No. 2022–3–23–083).

Appendix A. Supporting information

Supplementary data associated with this article can be found in the online version at doi:10.1016/j.apcatb.2023.122668.

References

[1] L. Kong, X. Tang, J. Zhu, Z. Wang, Y. Pan, H. Wu, L. Wu, Q. Wu, Y. He, S. Tian, Y. Xie, Z. Liu, W. Sui, L. Han, G. Carmichael, Improved inversion of monthly ammonia emissions in China based on the Chinese ammonia monitoring network and ensemble Kalman filter, Environ. Sci. Technol. 53 (2019) 12529–12538.
[2] X. Liu, Y. Zhang, W. Han, A. Tang, J. Shen, Z. Cui, P. Vitousek, J. Erisman, K. Goulding, P. Christie, A. Fangmeier, F. Zhang, Enhanced nitrogen deposition over China, Nature 494 (2013) 459–462.
[3] N. Roney, F. Llados, Toxicological profile for ammonia, U.S. Department of Health and Human Services Public Health Service, 2004.
[4] Y. Guo, M. Wen, G. Li, T. An, Recent advances in VOC elimination by catalytic oxidation technology onto various nanoparticles catalysts: a critical review, Appl. Catal. B: Environ. 281 (2021), 119447.
[5] Y. Guo, M. Wen, S. Song, Q. Liu, G. Li, T. An, Enhanced catalytic elimination of typical VOCs over $ZnCoO_x$ catalyst derived from in situ, Appl. Catal. B: Environ. 308 (2022), 121212.
[6] Z. Wang, P. Ma, K. Zheng, C. Wang, Y. Liu, H. Dai, C. Wang, H. Hsi, J. Deng, Size effect, mutual inhibition and oxidation mechanism of the catalytic removal of a toluene and acetone mixture over TiO_2 nanosheet-supported Pt nanocatalysts, Appl. Catal. B: Environ. 274 (2020), 118963.
[7] H. Jang, S. Xing, A model to predict ammonia emission using a modified genetic artificial neural network: analyzing cement mixed with fly ash from a coal-fired power plant, Constr. Build. Mater. 230 (2020), 117025.
[8] Y. Chang, Z. Zou, Y. Zhang, C. Deng, J. Hu, Z. Shi, A.J. Dore, J. Collett, Assessing contributions of agricultural and nonagricultural emissions to atmospheric ammonia in a Chinese megacity, Environ. Sci. Technol. 53 (2019) 1822–1833.
[9] K. Malook, H. Khan, M. Shah, Ammonia sensing behavior of polypyrrole-bimetallic oxide composites, Polym. Compos. 41 (2020) 2610–2615.
[10] F. Gao, Y. Liu, Z. Sani, X. Tang, H. Yi, S. Zhao, Q. Yu, Y. Zhou, Advances in selective catalytic oxidation of ammonia (NH_3-SCO) to dinitrogen in excess oxygen: A review on typical catalysts, catalytic performances and reaction mechanisms, J. Environ. Chem. Eng. 9 (2021), 104575.
[11] F. Wang, J. Ma, G. He, M. Chen, C. Zhang, H. He, Nanosize effect of Al_2O_3 in Ag/Al_2O_3 catalyst for the selective catalytic oxidation of ammonia, ACS Catal. 8 (2018) 2670–2682.
[12] M. Jabłońska, Progress on selective catalytic ammonia oxidation (NH_3-SCO) over Cu-containing zeolite-based catalysts, ChemCatChem 12 (2020) 4490–4500.
[13] M. Jabłońska, R. Palkovits, Copper based catalysts for the selective ammonia oxidation into nitrogen and water vapour-Recent trends and open challenges, Appl. Catal. B: Environ. 181 (2016) 332–351.
[14] Z. Qu, R. Fan, Z. Wang, H. Wang, L. Miao, Selective catalytic oxidation of ammonia to nitrogen over MnO_2 prepared by urea-assisted hydrothermal method, Appl. Surf. Sci. 351 (2015) 573–579.
[15] Y. Zhou, S. Rong, H. Xie, Y. Feng, D. Ding, W. He, N. Zhang, J. Lu, Enhancement of acidic sites in layered MnO_2 for the highly efficient selective catalytic oxidation of gaseous ammonia, J. Environ. Chem. Eng. 11 (2023), 109480.
[16] M. Chen, J. Ma, B. Zhang, F. Wang, Y. Li, C. Zhang, H. He, Facet-dependent performance of anatase TiO_2 for photocatalytic oxidation of gaseous ammonia, Appl. Catal. B: Environ. 223 (2018) 209–215.
[17] M. Chen, C. Zhang, H. He, Insights into designing photocatalysts for gaseous ammonia oxidation under visible light, Environ. Sci. Technol. 54 (2020) 10544–10550.
[18] Y. Li, S. Wu, J. Wu, Q. Hu, C. Zhou, Photothermocatalysis for efficient abatement of CO and VOCs, J. Mater. Chem. A 8 (2020) 8171–8194.
[19] J. Kong, G. Li, M. Wen, J. Chen, H. Liu, T. An, The synergic degradation mechanism and photothermocatalytic mineralization of typical VOCs over PtCu/CeO_2 ordered porous catalysts under simulated solar irradiation, J. Catal. 370 (2019) 88–96.
[20] P. Wu, S. Dai, G. Chen, S. Zhao, Z. Xu, M. Fu, P. Chen, Q. Chen, X. Jin, Y. Qiu, S. Yang, D. Ye, Interfacial effects in hierarchically porous α-MnO_2/Mn_3O_4 heterostructures promote photocatalytic oxidation activity, Appl. Catal. B: Environ. 268 (2020), 118418.
[21] D. Ding, Y. Zhou, T. He, S. Rong, Facet selectively exposed α-MnO_2 for complete photocatalytic oxidation of carcinogenic HCHO at ambient temperature, Chem. Eng. J. 431 (2022), 133737.
[22] Y. Bi, S. Ouyang, N. Umezawa, J. Cao, J. Ye, Facet effect of single-crystalline Ag_3PO_4 sub-microcrystals on photocatalytic properties, J. Am. Chem. Soc. 133 (2011) 6490–6492.
[23] X. Han, Q. Kuang, M. Jin, Z. Xie, L. Zheng, Synthesis of titania nanosheets with a high percentage of exposed (001) facets and related photocatalytic properties, J. Am. Chem. Soc. 131 (2009) 3152–3153.
[24] S. Rong, P. Zhang, F. Liu, Y. Yang, Engineering crystal facet of α-MnO_2 nanowire for highly efficient catalytic oxidation of carcinogenic airborne formaldehyde, ACS Catal. 8 (2018) 3435–3446.
[25] L. Wei, C. Yu, K. Yang, Q. Fan, H. Ji, Recent advances in VOCs and CO removal via photothermal synergistic catalysis, Chin. J. Catal. 42 (2021) 1078–1095.
[26] X. Zeng, C. Shan, M. Sun, D. Ding, S. Rong, Graphene enhanced α-MnO_2 for photothermal catalytic decomposition of carcinogen formaldehyde, Chin. Chem. Lett. 33 (2022) 4771–4775.
[27] P. Singh, V. Srivastava, Recent advances in visible-light graphitic carbon nitride (g-C_3N_4) photocatalysts for chemical transformations, RSC Adv. 12 (2022) 18245–18265.
[28] Q. Guo, C. Zhou, Z. Ma, X. Yang, Fundamentals of TiO_2 photocatalysis: concepts, mechanisms, and challenges, Adv. Mater. 31 (2019) 1901997.
[29] J. Kong, C. Jiang, Z. Rui, S. Liu, F. Xian, W. Ji, H. Ji, Photothermocatalytic synergistic oxidation: An effective way to overcome the negative water effect on supported noble metal catalysts for VOCs oxidation, Chem. Eng. J. 397 (2020), 125485.
[30] X. Guo, J. Li, Y. Wang, Z. Rui, Photothermocatalytic water splitting over Pt/$ZnIn_2S_4$ for hydrogen production without external heat, Catal. Today 402 (2022) 210–219.
[31] J. Li, J. Feng, X. Guo, H. Fang, J. Chen, C. Ma, R. Li, Y. Wang, Z. Rui, Defect-band bridge photothermally activates Type III heterojunction for CO_2 reduction and typical VOCs oxidation, Appl. Catal. B: Environ. 309 (2022), 121248.
[32] Y. Li, C. Wang, H. Zheng, F. Wan, F. Yu, X. Zhang, Y. Liu, Surface oxygen vacancies on WO_3 contributed to enhanced photothermo-synergistic effect, Appl. Surf. Sci. 391 (2017) 654–661.
[33] S. Yamazoe, T. Okumura, Y. Hitomi, T. Shishido, T. Tanaka, Mechanism of photo-oxidation of NH_3 over TiO_2: fourier transform infrared study of the intermediate species, J. Phys. Chem. C. 111 (2007) 11077–11085.
[34] Y. Shu, J. Ji, M. Zhou, S. Liang, Q. Xie, S. Li, B. Liu, J. Deng, J. Cao, S. Liu, H. Huang, Selective photocatalytic oxidation of gaseous ammonia at ppb level over Pt and F modified TiO_2, Appl. Catal. B: Environ. 300 (2022), 120688.
[35] F. Gao, S. Song, X. Tang, H. Yi, S. Zhao, Q. Yu, Tetraphenyl-porphyrin decorated anatase TiO_2 catalysts for the visible-light photocatalytic oxidation of gaseous ammonia at room temperature, Appl. Surf. Sci. 506 (2020), 144421.
[36] S. Yamazoe, K. Teramura, Y. Hitomi, T. Shishido, T. Tanaka, Visible light absorbed NH_2 species derived from NH_3 adsorbed on TiO_2 for photoassisted selective catalytic reduction, J. Phys. Chem. C. 111 (2007) 14189–14197.
[37] M. Lin, B. An, N. Niimi, Y. Jikihara, T. Nakayama, T. Honma, T. Takei, T. Shishido, T. Ishida, M. Haruta, T. Murayama, Role of the acid site for selective catalytic oxidation of NH_3 over Au/Nb_2O_5, ACS Catal. 9 (2019) 1753–1756.
[38] S. Zhang, Z. He, X. Li, J. Zhang, Q. Zang, S. Wang, Building heterogeneous nanostructures for photocatalytic ammonia decomposition, Nanoscale Adv. 2 (2020) 3610–3623.